Combined MEK and PI3K/p110b inhibition as a novel targeted therapy for malignant mesothelioma displaying sarcomatoid features

Miriam Marqués, Robin Tranchant, Blanca Risa-Ebrí, María Suárez-Solís, Luis Fernandez, Enrique Carrillo-De-Santa-Pau, Natalia del Pozo, Jaime Martínez de Villarreal, Clément Meiller, Yves Allory, et al.

Combined MEK and PI3K/p110β inhibition as a novel targeted therapy for malignant mesothelioma displaying sarcomatoid features

Miriam Marqués [1,2], Robin Tranchant [3,*], Blanca Risa-Ebrí [1], María L. Suárez-Solís[1,4], Luis C. Fernández [1], Enrique Carrillo-de-Santa-Pau[1,5], Natalia del Pozo [1,2], Jaime Martínez de Villarreal [1,2], Clement Meiller[3], Yves Allory [1,6], Yuna Blum[7], Christine Pirker[8], Balazs Hegedus [9], Simon T. Barry [10], Amancio Carnero [1,2,11], Walter Berger [8], Didier Jean [3], Francisco X. Real [1,2,12]

[1] Epithelial Carcinogenesis Group, Spanish National Cancer Centre-CNIO, Madrid, Spain

[2] CIBERONC, Madrid, Spain

[3] Centre de Recherche des Cordeliers, INSERM, Université Paris Descartes, Université Paris Diderot, Sorbonne Université, USPC, Functional Genomics of Solid Tumors team, F-75006 Paris, France.

[4] Department of Surgical Pathology, Hospital Clínico San Carlos, Madrid, Spain.

[5] Computational Biology Group, Precision Nutrition and Cancer Research Program. IMDEA Food Institute. Madrid, Spain

[6] Université Paris-Est Créteil, France INSERM, U955, Institut Mondor de Recherche Biomédicales AP-HP, Hôpital Henri Mondor, Department of Pathology, Créteil, France

[7] Programme Cartes d'Identité des Tumeurs (CIT), Ligue Nationale Contre Le Cancer, Paris, France

[8] Institute of Cancer Research and Comprehensive Cancer Center, Medical University Vienna, Austria

[9] Department of Thoracic Surgery, Medical University Vienna, Austria

[10] IMED Oncology, AstraZeneca, Li Ka Shing Centre, Cambridge

[11] Instituto de Biomedicina de Sevilla, IBIS/HUVR/ Universidad de Sevilla/ Consejo Superior de Investigaciones Científicas; Avda. Manuel Siurot s/n 41013, Sevilla, Spain

[12] Departament de Ciències Experimentals i de la Salut, Universitat Pompeu Fabra, Barcelona, Spain

[*] Present address: Laboratoire de Biochimie (LBC), ESPCI Paris, PSL Research University, CNRS UMR-8231, Chimie Biologie Innovation, Paris, France.

Keywords: sarcomatoid mesothelioma, PI3K, MAPK, GPCRs

Running title: Targeted therapies for sarcomatoid malignant mesothelioma

Financial Support: This work was supported, in part, by grants from Asociación Española Contra el Cáncer (FXR), Spanish Ministry of Economy and Competitivity, Plan Estatal de I+D+I 2013-2016, ISCIII (FIS PI15/00045) (AC), RTICC (Instituto de Salud Carlos III, grants RD12/0036/0034 to FXR and AC, respectively), and CIBERONC (CB16/12/00453 and CD16/12/00275 to FXR and AC, respectively), co-funded by FEDER from Regional Development European Funds (European Union) and Inserm (Institut national de la santé et de la recherche médicale). MM was supported by a Sara Borrell Fellowship from Instituto de Salud Carlos III. CNIO is supported by Ministerio de Ciencia, Innovación y Universidades as a Centro de Excelencia Severo Ochoa SEV-2015-0510.

Corresponding authors: Francisco X. Real and Miriam Marqués, Epithelial Carcinogenesis Group, Spanish National Cancer Research Centre-CNIO, Madrid, 28029, Spain. E-mails: freal@cnio.es, mmarques@cnio.es

Competing interests: The authors state that they have no conflict of interest to disclose.
Word count main text: 5019

Figures: 7 main Figures, 7 Supplementary Figures.

Statement of significance: Mesothelioma is highly aggressive; its sarcomatoid variants have worse prognosis. Building on a genetic mouse model, a novel combination therapy is uncovered that is relevant to human tumors.

Abstract

Among malignant mesotheliomas (MM) the sarcomatoid subtype is associated with higher chemoresistance and worst survival. Due to its low incidence, there has been little progress in the knowledge of the molecular mechanisms associated with sarcomatoid MM, which might help to define novel therapeutic targets. In this work, we show that loss of PTEN expression is frequent in human sarcomatoid MM and PTEN expression levels are lower in sarcomatoid MM than in the biphasic and epithelioid subtypes. We confirm that combined *Pten* and *Trp53* deletion in mouse mesothelium leads to non-epithelioid MM development. In *Pten;Trp53*-null mice developing MM, the Gαi2 coupled receptor subunit drives MEK/ERK and PI3K activation, resulting in aggressive, immune-suppressed tumors. Combined inhibition of MEK and p110β /PI3K reduces mouse tumor cell growth *in vitro*. Therapeutic inhibition of MEK and p110β /PI3K using Selumetinib (AZD6244, ARRY-142886) and AZD8186, two drugs that are currently in clinical trials, increases the survival of *Pten;Trp53*-null mice without major toxicity. This drug combination effectively reduces the proliferation of primary cultures of human pleural (Pl) MM, implicating non-epithelioid histology and high Vimentin, AKT1/2, and Gαi2 expression levels as predictive markers of response to combined MEK and p110β/PI3K inhibition. Our findings provide the rationale for the use of Selumetinib and AZD8186 in MM patients with sarcomatoid features. This constitutes a novel targeted therapy for a poor prognosis and frequently chemoresistant group of MM patients, for whom therapeutic options are currently lacking.

Introduction

Malignant Mesothelioma (MM) arises mainly from the pleural (pl) and peritoneal (pe) mesothelium and less frequently from other sites and it is strongly associated with asbestos exposure. There are three main histologic subtypes: epithelioid (EMM), accounting for approximately 60% of MM; sarcomatoid (SMM), constituting approximately 20%; and biphasic (BMM). BMM contain a variable proportion of tumor cells with epithelioid and sarcomatoid features. Patients with MM have an extremely poor prognosis, especially when the tumor displays sarcomatoid features (pure or biphasic), in part due to its aggressiveness and chemoresistance. Even with multimodality treatment, median survival is 14-18 months (1). There is currently no standard second-line treatment for MM and Bevacizumab is the only approved targeted therapy, in combination with cisplatin and pemetrexed (2). This is due, in part, to the limited understanding of the molecular pathogenesis of MM. Genetic analyses have allowed classifying MM and identifying druggable pathways (3-7). Sarcomatoid MM cases are underrepresented in all reported cohorts, constituting 3-9% of all specimens, hampering their molecular characterization and the identification of genetic alterations contributing to their poor prognosis and chemoresistance. Recently proposed molecular classifications of MM agree on the existence of a poor prognosis subtype which includes sarcomatoid tumors. *TP53* alterations and PI3K-mTOR and RAS/MAPK upregulation were proposed to associate with the non-epithelioid clusters (6-8).

The PI3K/AKT/mTOR pathway promotes cell proliferation and survival and is activated in most MM (9-11). The mechanisms leading to PI3K/AKT/mTOR activation have not been completely elucidated. Point mutations in genes coding for PI3K pathway components are rare in MM (6,12) but loss of expression of PTEN, the lipid phosphatase that dephosphorylates the main PI3K product [PtdIns(3,4,5)P3] (PIP3), appears much more frequent (16-62%) measured by immunohistochemical assays (13-16). Genetic MM mouse models, sometimes combined with asbestos exposure, have confirmed the key role of PI3K/mTOR activation and *Trp*53 inactivation in MM initiation and progression (17-19).

Indeed, combined *Pten* and *Trp53* deletion in mouse pleural or peritoneal mesothelium leads to sarcomatoid and biphasic MM (19).

PI3K members belong to three classes; class I PI3K are subdivided into IA and IB based on their structure and the activating mechanisms. Class IA PI3K members are heterodimers of a catalytic (p110) and a regulatory subunit (p85). Four genes (*PIK3CA*, *PIK3CB*, *PIK3CD*, and *PIK3CG*) code for individual p110 isoforms (p110α, p110β, p110γ , p110δ). p110α and p110β are ubiquitous while p110δ and p110γ expression is enriched in hematopoietic cells. p110α signals downstream of receptor tyrosine kinases (RTKs) while p110β has a prominent role downstream of GPCRs (20,21). PIP3 activates AKT which, in turn, signals to mTOR via TSC1/2 phosphorylation.

Here we report that concurrent PI3K activation and *Trp53* deletion in the peritoneal mesothelium leads to aggressive sarcomatoid MM, confirming previous findings (19). We find that *Pten* deletion drives more aggressive tumors than *Pik3ca* mutational activation. We confirm that human SMM display low PTEN expression. These mouse model-based strategies allowed identifying the mechanisms responsible for the aggressiveness of SMM, which revealed combined p110β/MEK inhibition as a novel targeted therapy for MM with sarcomatoid features.

Materials and Methods

Mouse strains. $Pten^{lox/lox}$ and $Trp53^{lox/lox}$ strains were previously reported (22,23). To generate $Pik3ca^{H1047R}$ knockin mice, the *Pik3ca* region encompassing exon 18 to 3'UTR, comprising exons 18-20, was substituted by homologous recombination by a cDNA including wild type exons 18-20-3'UTR followed by PGK-NEO for Neomycin selection. These sequences were flanked by LoxP sites; following the 3' LoxP site, the recombinant sequence included the cDNA of exons 18-20 with the 3141A<G substitution, coding for the H1047R mutation, followed by IRES GFP-Luc, and the 3'UTR (Fig. 1A). The construct was electroporated into embryonic stem cells (ESC), which were selected with neomycin. The recombinant sequence was analyzed by PCR. Positive cells were transferred into pseudo-pregnant female

mice. ESC electroporation, selection and transfer followed standard protocols. Mice born after ESC transfer were genotyped by Southern blot and PCR, crossed with wild-type (WT) C57BL/6 mice, and pups were genotyped to verify germ line transmission. Mice from all the indicated strains (mixed background) were bred and maintained in specific pathogen-free conditions. All animal procedures were approved by the Ethics Committee for Research and Animal Welfare of Instituto de Salud Carlos III and the General Guidance of the Environment of Madrid Community and performed following guidelines for Ethical Conduct in the Care and Use of Animals as stated in The International Guiding Principles for Biomedical Research involving Animals, developed by the Council for International Organizations of Medical Sciences.

Histopathology, immunohistochemistry, and RNAscope. Mouse tissues were dissected, fixed in 10% buffered formalin, and paraffin-embedded. Human MM tissue microarrays (TMAs) and associated data were obtained through the National Mesothelioma Virtual Bank (University of Maryland, MD; University of Pittsburgh Medical Center, PA; and Roswell Park Cancer Institute, NY, USA). Antigen retrieval was performed by boiling in citrate buffer pH 6.0; endogenous peroxidase was inactivated with 3% H_2O_2 in methanol. Sections were blocked, rinsed, and incubated with specific antibodies (Supplementary Table S1) and species-specific secondary HRP-conjugated antibodies (EnVision™ Systems, DAKO-Agilent Technologies). Reactions were developed using DAB (DAKO-Agilent Technologies). Histoscores of human TMAs were calculated as the product of the proportion of reactive cells (0-100%) and intensity (0-3). The average of the histoscores from each patient was used for analysis. RNAscope *in situ* hybridization for PD-L1 and Ppib (used for quality control) on formalin-fixed paraffin-embedded mouse tumors were performed using the RNAscope 2.5 HD Assay-RED (Advanced Cell Diagnostics) according to manufacturer's instructions. For mouse immunohistochemistry and RNAscope quantification, hematoxylin and antigen-specific signals were detached into separated channels by Colour Deconvolution plugin of Image J software and channel-specific pixel area quantified using the same

software. DAB area was normalized to the hematoxylin area; PD-L1 RNAscope signal was normalized to *Ppib* signal.

Western blotting (WB) and protein-based assays. Frozen tissues and cultured cells were lysed in radioimmunoprecipitation buffer (20mM Tris-HCl, pH 8.0, 137 mM NaCl, 1 mM $MgCl_2$, 1 mM $CaCl_2$, 10% glycerol, 1% NP40, 0.5% sodium deoxycholate, 0.1% sodium dodecyl sulfate [SDS]) containing protease and phosphatase inhibitors. Proteins fractionated by SDS-PAGE were transferred to nitrocellulose membranes, which were incubated with primary antibodies (Supplementary Table S1) and HPRP-conjugated secondary antibodies (DAKO-Agilent Technologies). Reactions were developed using Luminata Classico HRP substrate (Merck-Millipore). Phospho-RTK array (R&D Systems); RAS Activation Assay kits (Merck-Millipore) were used following manufacturer's guidelines. Image J software was used for WB signal quantification.

RNA analysis: SNaPshot, and RT-qPCR. Total RNA was isolated from frozen tissues and cultured cells using GenElute Mammalian Total RNA Miniprep Kit (Sigma-Aldrich). DNA was eliminated using the DNA-free kit (Ambion-Life Technologies). Reverse transcription was performed using TaqMan® reverse transcription reagents (Roche-Life Technologies); for PCR, an ABIPRISM 7900HT instrument (Applied Biosystems-Life Technologies) and the SYBR Green PCR Master Mix (Applied Biosystems-Life Technologies) were used. Changes in gene expression were calculated using the quantitative ΔΔCt method and normalized against *Hprt*. To assay for expression of mutant *Pik3ca* mRNA, a region of the gene encompassing exons 19 and 20 was amplified by PCR from cDNA. PCR products were treated with ExoSAP-IT (Affymetrix-Thermo Fisher Scientific) and the wt and the H1047R alleles were identified using a specific primer and the ABI PRISM SNaPshot Multiplex Kit (Applied Biosystems-Life Technologies). All primer sequences are provided in Supplementary Table S2.

RNA-sequencing. Total RNA (2 µg) from *Pik3ca*;Trp53*-null and *Pten;Trp53*-null mice (n=6 each) was used. RNA Integrity Numbers ranged from 7.5-9.4, assayed on an Agilent 2100 Bioanalyzer. PolyA+ RNA was extracted and randomly fragmented, converted to double stranded cDNA, and

processed through enzymatic treatments of end-repair, dA-tailing, and adapter ligation following "TruSeq RNA Sample Preparation Guide". The library was produced by limited-cycle PCR with Illumina PE primers (8 cycles). The purified cDNA library was applied to an Illumina flow cell for cluster generation (TruSeq cluster generation kit v5) and sequenced on the Genome Analyzer IIx with SBS TruSeq v5 reagents.

RNA-seq data processing and analyses. Image analysis and per-cycle base-calling was performed with Illumina Real Time Analysis software (RTA1.13). Conversion to FASTQ read format with the ELAND algorithm (v2e) was performed with CASAVA-1.8 (IlluminaQuality check was done via fastqc v0.9.4, Babraham Bioinformatics). Raw reads were aligned with Tophat5 (version 2.0.4) to mouse genome GRCm38/mm10. Gene expression normalized counts (TPMs) and differential expression (*Pik3ca*;Trp53*-null vs. *Pten;Trp53*-null mice) was done with DeSeq2 (version 2.0.2).

MM transcriptome data. RNAseq data (6) were downloaded from the European Genome-phenome Archive under accession code EGAS00001001563; data were normalized by the Upper Quartile method. Normalized data from the TCGA were downloaded from cBioPortal for Cancer Genomics (24).

Cell culture. For mouse tumor cell isolation, tumors were digested in NB8 collagenase (1.5 mg/mL in HBSS) (LabClinics) and maintained in DMEM supplemented with 10% FBS, 1mM Na pyruvate and non-essential amino acids (Gibco-Life Technologies), and incubated at 37 ºC in a 5% CO_2 and 3% O_2 atmosphere. All experiments were performed at <15 passage. Human primary mesothelioma cultures (MPM.04, 12, 24, 28, 29, 34, 35, 37, 47, 59 and 60) were established at INSERM U.1138. MESO.49, 62, 80, 84, 92, 103, 161 and VMC.40, 48 were established at the Medical University of Vienna. Cells were grown either in RPMI 1640 (VMC40 and Meso161) or in DMEM supplemented with Glutamax (Gibco-Life Technologies) and 10% FBS at 37 ºC in a 5% CO_2 atmosphere.

Reagents and antibodies. PD0325901 MEK inhibitor (1408) was purchased from Axon-Medchem, TGX-221 (S1169) was obtained from Selleckchem, Pertussis toxin (P7208) and Cisplatin

(C2210000) were from Sigma-Aldrich (P7208). Selumetinib and AZD8186 were kindly provided by AstraZeneca.

In vitro invasion and proliferation assays. In vitro invasion assays were performed using BioCoat™ Matrigel™ Invasion Chambers (Corning) following manufacturer's guidelines. Cells were fixed with 4% PFA and nuclei were stained with DAPI (0.5μg/mL in PBS). Cells were visualized using a Leica TCS SP5 WLL confocal microscope. IMARIS software v5.0 (Bitplane) was used for 3D image reconstruction and nuclear quantification. Mouse cell proliferation assays were performed in 96-well plates (Greiner Bio-one). 24h after plating at $5x10^3$ cells/well (triplicates), inhibitors or vehicle were added; cells were incubated until fixation with 4% PFA. Visualization and image acquisition of DAPI stained nuclei were performed using the confocal microscopy-based PerkinElmer's Opera® high content screening system. Nuclei were counted using Acapella software (PerkinElmer). For proliferation assays, human primary cells were seeded at $5\text{-}7x10^3$ cells/well in triplicate in 96-well plates (Corning, Falcon). Cells were treated for 72 h with increasing concentrations of single, or both, drugs; viability was quantified by CellTiter 96 AQueous One Solution Cell Proliferation Assay (MTS) (G3582) or CellTiter Glo Luminescent Cell Viability Assay (G7573) (Promega). The combination ratios for Selumetinib and AZ8186 are specified in Supplementary Table S3. Area Under Curve (AUC) and GI50s for single drugs were calculated using GraphPad software 5.0 (Prism). Combination drug GI50 and CI were determined by Compusyn software (http://www.combosyn.com/).

Lentiviral production and Gαi2 knockdown. Gαi2 was knocked-down in mouse mesothelioma cells using MISSION shRNA Gαi2-shRNAs (SHC002, SHCLNG-NM_008138, and control sh; Sigma Aldrich). Targeting sequences are provided in Supplementary Table S2. Lentiviruses were produced in 293T cells using calcium phosphate transfection. Viral supernatant was collected 48h and 72h after transfection. Lentiviruses were transduced into mouse mesothelioma cells (0.2x106 cells /6 well-plate) followed by Puromycin selection (1μg/ml, 48h). Cells were harvested 24 hours later.

In vivo experiments. CT tumor-bearing *Pten;Trp53*-null mice were randomized into control and treatment groups. Selumetinib (10mg/kg) and AZD8186 (40mg/kg) were administered by oral gavage, twice daily, 5 days/week. Control mice received vehicle (0.5% methylcellulose, 0,2% Tween80).

MicroCT imaging. Mice were anesthetized and the abdominopelvic area was imaged using the eXplore Vista micro-CT scanner (GE Healthcare) without contrast. Micro-CT image acquisition consisted of 400 projections collected in one full rotation of the gantry in approximately 10 min using 80 kV and 450 µA X-ray tube settings. Reconstructed images were viewed and analyzed using AMIDE software.

Statistical analyses. Mann-Whitney U-Test was used to compare differences between two independent groups when the data did not follow a normal distribution. Kruskal-Wallis one-way analysis of variance was used when more than two groups were compared. Log-rank (Mantel-Cox) test was used to compare survival distributions. Fisher's exact test was used in the analysis of the distribution of categorical values within two groups. GraphPad software 5.0 (Prism) was used. Human data statistics were performed by R software, ANOVA test was used to compare differences between group means, and Tukey Test was applied as post-hoc test. Two-sided P values <0.05 were considered significant.

Results

Trp53 loss cooperates with both Pik3ca mutation and Pten loss in mouse MM. Peritoneal MM developed in 8-12 week-old *Pten*$^{lox/lox}$*;Trp53*$^{lox/lox}$ mice (referred to herein as *Pten;Trp53*-null) following inoculation of adenoviruses coding for Cre-recombinase into the bladder wall, as described (Fig. 1B, Supplementary Information) (18). Recombination was evaluated using *R26-LSL-LacZ* reporter mice two weeks later (Fig. 1C, Supplementary Information). All inoculated *Pten;Trp53*-null mice (n=26), but only 2/11 *Trp53*$^{lox/lox}$ mice, developed tumors in the peritoneal aspect of the bladder wall, frequently invading contiguous fat and muscle (Fig. 1D). In addition, 15/26 (57%) mice developed peritoneal lesions. Tumor histology and latency recapitulate previously described *Trp53;Pten*-null non-epithelioid MM (19). Tumors were pleomorphic, enriched in spindle-cells, and showed mild infiltration by lymphocytes and granulocytes. Immunohistochemistry showed heterogeneous but consistent expression of WT1 (9/9) and

vimentin (12/12) and diffuse KRT5 expression in 4/12 tumors (Fig. 1E). These features, together with the histology, are characteristic of SMM.

Given the relevance of the PI3K/AKT/mTOR pathway in MM cell proliferation and survival (9,10,18) we assessed more broadly the impact of PI3K activation in a *Trp53*-null context. We analyzed *Pik3ca*$^{wt/H1047R}$*;Trp53*$^{lox/lox}$ mice (referred to as *Pik3ca*;Trp53*-null), in which the H1047R hotspot mutation was conditionally knocked in the *Pik3ca* locus (Fig. 1A). After adeno-Cre inoculation, all *Pik3ca*;Trp53*-null mice developed tumors histologically undistinguishable from those of *Pten;Trp53*-null mice (Fig. 1E). However, the median survival of *Pik3ca*;Trp53*-null mice was significantly longer than that of *Pten;Trp53*-null mice (17.6 vs. 10.9 weeks after adenoviral inoculation, $P<0.0001$) (Fig. 1F). Importantly, <20% of *Pik3ca*;Trp53*-null mice (n=24) developed macroscopic metastases (intraperitoneal, spleen, kidneys, liver and gastrointestinal tract), compared with 50% of *Pten;Trp53*-null mice (n=14) ($P=0.024$, Fisher´s exact test) (Supplementary Fig.S1).

Immunohistochemical analysis revealed that *Pten;Trp53*-null tumors displayed higher proliferation (phospho-Histone 3) and increased inflammation (macrophages and T cells) than *Pik3ca*;Trp53*-null tumors; with no differences in apoptosis (cleaved-Caspase 3) (Fig. 2). A refined analysis revealed increased $Cd8^+$ cells, $Ym1^+$ M2 macrophages, and $Cd4^+$ $FoxP3^+$ T regs in *Pten;Trp53*-null tumors (Fig. 2C and D). RNAscope analysis showed discrete areas of PD-L1-expressing cells in *Pten;Trp53*-null tumors, but not in *Pik3ca*;Trp53*-null lesions (Fig. 2E and F). These data indicate that *Pten* inactivation associates with a more immunosuppressive stroma and metastatic phenotype than *Pik3ca* activation.

Human SMM display low PTEN expression. Given the relevance of *Trp53* inactivation and PI3K activation in mouse SMM, we interrogated the PI3K pathway and upstream regulators in human SMM. PTEN loss, assesed by immunohistochemistry, has been reported in 12-62% of unselected MM (11,13-15) but its relevance to the sarcomatoid phenotype is unknown. PTEN expression was analyzed in TMAs including 149 clinically annotated specimens (National Mesothelioma Virtual Bank, Supplementary Table

S4) (25). PTEN immunostaining scores were categorized as negative (0), weak (1), moderate (2), and strong (3) (Fig. 3A): 15.4% tumors scored negative (<20 immunoscore). PTEN-negative cases were enriched in SMM (*P*=0.017, Fisher's exact test) (Fig. 3B). PTEN immunoscores were significantly lower in SMM than in epithelioid and biphasic tumors (Fig. 3C). Given the heterogeneity of biphasic MMs, we subdivided them according to the sarcomatoid or epitheliod components. Biphasic MMs with <50% epithelioid cells displayed lower PTEN levels but differences were not significant when compared with those with >50% cells (*P*=0.134). At the transcriptomic level, expression of PTEN was significantly lower in the sarcomatoid group of Bueno (6), while expression of other PI3K effectors was increased. Despite following the same trend, differences were not significant when considering histology groups (Fig. 3D). A similar tendency was observed in the TCGA cohort (7) when clustered similarly (6) (Fig 3E). These data demonstrate that PTEN down-regulation is common in SMM and validate the *Pten;Trp53*-null mouse model as a valuable tool.

MEK/ERK activation contributes to the growth and invasive capacity of Pten;Trp53-null tumor cells. To identify the mechanisms contributing to the aggressiveness of *Pten;Trp53*-null tumors, we analyzed PI3K and MAPK/ERK activation, known to cooperate in tumor progression. Akt Ser473 and Thr308 phosphorylation was significantly higher in *Pten;Trp53*-null tumors compared with *Pik3ca*;Trp53*-null tumors. Remarkably, pErk1/2 (Thr202 and Tyr204) and pMek1/2 (Ser217/221) were also higher in *Pten;Trp53*-null tumors (Fig. 4A-C). We used RAS-GTP pull-down assays to assess upstream signaling and did not find strong evidence of RAS hyperactivation in *Pten;Trp53*-null tumors, compared with *Pik3ca*;Trp53*-null tumors (Supplementary Fig. S2A and S2B). Downstream, we did not find consistent differences in phosphorylation of GSK3β Ser9 nor in the mTOR targets S6K and 4Ebp1 in *Pten;Trp53*-null tumors (Supplementary Fig. S2C and S2D).

To study the mechanisms involved in MEK/ERK activation and their contribution to the aggressiveness of *Pten;Trp53*-null tumors, we established murine MM cell lines (Fig. 4D). Expression of mutant *Pik3ca* mRNA in *Pik3ca*;Trp53*-null cells was confirmed using a SNaPshot assay

(Supplementary Fig. S3A). *Trp53* and *Pten* deletion were also confirmed (Fig. 4E and Supplementary Fig. S3B). We found higher pAkt levels in *Pten;Trp53*-null cells than in *Pik3ca*;Trp53*-null cells (Fig. 4E and Supplementary Fig. S3C) but the differences in pERK levels in exponentially growing cells from both genotypes were less apparent than in tumor tissues. MEK1/2 inhibition with PD325901 led to decreased pErk in cells of both genotypes (Supplementary Fig. S4A). MEK1/2 inhibition led to reduced *in vitro* proliferation and invasiveness of *Pten;Trp53*-null cells whereas only proliferation was affected in *Pik3ca*;Trp53*-null cells (Fig. 4F and 4G). These results indicate that MAPK pathway activation contributes to the aggressiveness of *Pten;Trp53*-null tumors, although additional signaling pathways must be implicated.

GPCRs mediate Erk and PI3K activation in Pten;Trp53-null tumor cells. MAPK activation resulting from PTEN loss has been reported but no underlying unifying mechanism has been identified (26). A role of RTK - such as EGFR, EpHB4, MET and AXL - in MAPK activation has been proposed in MM (10,27). To explore if such mechanisms are involved in the differential activation of MAPK in *Trp53;Pten*-null mice, tumor lysates were analysed by p-RTK dot blot arrays. We did not find strong evidence for a role of hyperphosphorylation of any of the 39 RTK tested. By contrast, selected receptors were preferentially hyperphosphorylated in *Pik3ca*;Trp53*-null tumors (Fig. 5A and 5B). Altogether, these results do not support RTK/RAS as the predominant mechanism responsible for MAPK activation in aggressive *Pten;Trp53*-null MM.

Next, we assessed whether GPCRs may participate in MAPK activation. To explore this notion, we used Pertussis toxin (PTX) which induces ADP-ribosylation of the αi subunits of heterotrimeric G proteins and impaired interaction with GPCRs, thus preventing downstream pathway activation (28). Erk phosphorylation was markedly reduced in PTX-treated *Pten;Trp53*-null cells but not in *Pik3ca*;Trp53*-null cells while Akt phosphorylation was only modestly affected (Fig. 5C). The Gαi family consists of Gαi1-3, Gαo, Gαt1-3, and Gαz. RNA-Seq data showed that Gαi2 is the main Gαi subunit expressed in mouse SMM, regardless of the host genotype (Fig. 5D). Gαi2 expression was confirmed at the protein

level in all tested *Pten;Trp53*-null (n=8) and *Pik3ca*;Trp53*-null (n=9) MM by immunohistochemistry, with a heterogeneous expression pattern (Fig. 5E). To confirm the role of GPCRs signaling in MAPK activation in *Pten;Trp53*-null cells, we targeted Gαi2 using shRNAs. Gαi2 knockdown efficiently and consistently reduced Erk and Akt phosphorylation in *Pten;Trp53*-null, but not in *Pik3ca*;Trp53*-null cells (Fig. 5F). These results provide novel evidence on the involvement of GPCRs in MAPK and PI3K activation in *Pten;Trp53*-null MM cells. To further assess the relevance of this pathway in human MMs, we interrogated expression in the series from Bueno et al. (6), finding that GNAI2 expression is significantly up-regulated in sarcomatoid transcriptome- and histology-defined subgroups (Fig. 5G).

P110β and Mek1/2 inhibitors cooperate to suppress mouse Pten;Trp53-null tumors growth. p110β has been shown to play a crucial role in PTEN-null tumors *in vitro* and *in* vivo (29,30) and is mainly activated by GPCRs (21). We hypothesized that p110β and Mek1/2 cooperate driving the aggressive phenotype of *Pten;Trp53*-null tumors. TGX-221, a selective p110β inhibitor, reduced PI3K-dependent Akt phosphorylation (Thr308) to a greater extent in *Pten;Trp53*-null cells than in *Pik3ca*;Trp53*-null cells. Surprisingly, mTORC2-dependent phosphorylation of Akt (Ser473) was inhibited in all cell lines (Supplementary Fig. S4B). TGX-221 had no effect on pErk, suggesting that combined inhibition of p110β and MEK1/2 might be more active in *Pten;Trp53* cells.

As single agents, TGX-221 and PD325901 had modest anti-proliferative effect. However, their combination completely suppressed the proliferation of *Pten;Trp53*-null cells. Both inhibitors decreased *in vitro* invasiveness (Fig. 6A and 6B). Based on the *in vitro* efficacy of simultaneous MEK and p110β inhibition, we tested the combination *in vivo* using drugs undergoing clinical investigation. Selumetinib is a selective MEK1/2 inhibitor in phase III trials for NSCLC, thyroid cancer, and metastatic uveal melanoma and AZD8186 is a p110β/p110δ inhibitor undergoing phase I investigation (https://clinicaltrials.gov). *Pten;Trp53*-null tumor growth was followed by weekly micro-CT; early tumor detection was facilitated by bone differentiation, a common feature of MM (Fig. 6C). Once tumors were detected (6-7 weeks after Cre inoculation), mice (n=6/group) were randomized to receive daily oral

treatment with vehicle, Selumetinib, AZD8186, or Selumetinib/AZD8186 for 7 weeks. Single compound treatment did not affect survival. In contrast, a significant lifespan increase (*P*=0.031) was observed with the combination (Fig. 6D)**.** Accordingly, CT images showed increased size and number of lesions in vehicle- and single compound-treated mice, and reduced tumor progression upon drug combination (Fig. 6E)**.** The dependency of tumor shrinkage on treatment was shown upon its discontinuation: within the following 5 weeks, tumors grew in 5 mice but one surviving mouse sacrificed 26 weeks later showed a complete pathological response (Supplementary Fig. S5A and S5C)**.** In an independent experiment, CT tumor-bearing *Pten;Trp53*-null mice were randomized to receive vehicle or Selumetinib/AZD8186 (n=11). Treatment was maintained for 12 weeks without toxicity. Median survival of treated *Pten;Trp53*-null mice was 13.4 weeks, compared with 9.3 weeks for control mice (*P*=0.005) (Fig. 6F). Of two surviving mice, one had a minimal peritoneal tumor and the other displayed only microscopic tumor foci at autopsy (Supplementary Fig. S5B, S5D and S5E).

P110β and Mek1/2 inhibitors cooperate to suppress human pl-MM cell growth. We next analyzed the effects of this drug combination on 20 human primary pl-MM cultures [EMM (n= 8), BMM (n=7) and SMM (n=5)] (4,31-33). Unfortunately, no primary pe-MM were available for these studies. Response was defined as a >50% reduction of cell viability and combination GI50 <10μM (calculated as the sum of GI50s of each drug). Six of 12 BMM/SMM and 1/8 EMM cultures responded to the combination (Fig. 7A, 7B, and Supplementary Fig. S6A); in 6 of the responding cultures Selumetinib and AZD8186 were synergistic, displaying a combination index (CI) <1 (Supplementary Table S5). BMM and SMM also displayed lower GI50s to Selumetinib/AZD8186 combination (Supplementary Fig. S6B and S6C). AUC responses to increasing drug concentrations revealed that BMM and SMM were more sensitive to AZD8186 (*P*=0.015), and to the combination (*P*=0.049), than EMM (Fig. 7B and 7C). To further define predictive markers of response to the Selumetinib/AZD8186 combination, we assessed Vimentin, Gαi2, TP53, and MAPK and PI3K pathways status in lysates from primary human MM cells (Fig. 7D) and found that low Vimentin, Gαi2, and AKT levels identify the subgroup of resistant cells (Fig 7E). Finally,

to explore the potential clinical relevance of these findings, we compared the effects of Selumetinib/AZD8186 combination to cisplatin (Supplementary Fig. S7): responder cells displayed higher sensitivity to Selumetinib/AZD8186 than to cisplatin (P=0.038) (Fig. 7F). Altogether these results point to Selumetinib/AZD8186 as a novel therapy alternative to Cisplatin for pl- an pe- non-epithelioid MM patients, high expression of Vimentin, AKT, and Gαi2 being candidate biomarkers predictive of response.

Discussion

There is an urgent need to understand the molecular factors linked to sarcomatoid MM subtype and their aggressiveness to define therapeutic improvements. EMT may, in part, explain the poor prognosis of SMM, conferring both high invasiveness and chemoresistance (4,6,7). Recent reports highlight genetic alterations and molecular mechanisms associated to EMT in SMM, such as *TP53* inactivation, *LATS2* mutations, *CDKN2A* homozygous deletions, E2F target up-regulation, lncRNA expression, and PI3K-mTOR and RAS/MAPK activation (4,6,7,34). Here, we confirmed the relevance of concomitant *Trp53* loss and PI3K activation as drivers of mouse SMM. A few genetic models of MM have previously been reported based on the inactivation of *Nf2*, *Bap1*, *Ink4a/Arf*, *Trp53*, *Tsc1* and *Pten* - with or without the combined administration of asbestos. In most cases, the 3 major histological subtypes of MM developed but only *Nf2;Rb* and *Pten;Trp53* combined genetic loss leads to exclusively non-epithelioid (17,19,35). In our hands, adenovirus-Cre mediated *Pten;Trp53* inactivation resulted in SMM development with a median latency and histology similar to those reported by Sementino *et al.* but we did not observe biphasic MM, as they did. These differences might reside in the genetic background used.

PI3K/AKT/mTORC1 and ERK pathway activation occurs in most human MM specimens, thought to be a consequence of RTK activation (9,10,18), although anti-RTKs therapies have shown limited effectiveness (16,36). The role of PTEN, and its implication in PI3K pathway activation in MM, is controversial as few genetic alterations have been identified in this gene. However, *PTEN* can be inactivated through multiple mechanisms (37). Thus, PTEN loss has been reported in 16-62% of cases using immunohistochemistry (11,13-15) and a recent case report associates PTEN-hamartoma-tumor-

syndrome with MM development pointing to PTEN loss as a MM driver (38). Most studies relating PTEN and MM did not discriminate between histologic MM subtypes. We show using human MM TMAs that PTEN protein loss is frequent in SMM and that this subtype displays lower PTEN expression, compared with epithelioid and biphasic MM. The analysis is limited by the low number of sarcomatoid samples in our cohort (n=7) but *PTEN* mRNA levels were lower in transcriptomic defined sarcomatoid tumors when compared with the other MMs. PTEN expression in biphasic MMs is paradoxal, with higher histoscores in sarcomatoid tumors. Biphasic MM constitutes a highly heterogeneous group with variable proportions of epithelioid and sarcomatoid cells. These differences were highlighted in the transcriptomic Biphasic-E and Biphasic-S clusters defined by Bueno et al. (6). In addition, the relevance of intratumor heterogeneity regarding epithelioid and sarcomatoid components was recently underscored by Blum et al. (8), indicating that a more precise definition of the biphasic group is required. The reported low PTEN levels in sarcomatoid MMs, plus the reported association of TP53 mutations with non-epithelioid MM, underline the relevance of *Trp53;Pten*-null mice as a MM pre-clinical model (6,8,19).

Our data also revealed that *Pten* loss has stronger oncogenic properties than *Pik3ca* mutations, favoring metastases and an immunosuppressive environment enriched in Cd8 T cells, T regs, M2 macrophages, and PD-L1-expressing cells that have been associated with poor prognosis in human MM (39-41). Remarkably, non-epithelioid human MMs exhibit higher PD-L1 expression and T cell infiltration (6-8,41). These observations are in agreement with the fact that PTEN antagonizes further PI3K isoforms implicated in the activation of pathways other than mTOR, and that it exerts lipid phosphatase-independent functions (42). Biochemical analysis of *Pik3ca*;Trp53*-null and *Trp53;Pten*-null tumors revealed strong Akt and Mek/Erk activation without major evidence for a role of upstream RTKs. This allowed us to uncover a novel role of GPCR/Gαi2 signaling in Erk phosphorylation specifically in *Trp53;Pten*-null, but not in *Pik3ca*;Trp53*-null, cells. Importantly, Gαi2 mRNA levels are upregulated in human sarcomatoid MMs when compared with the other subgroups and its signaling has been implicated in the proliferation and migration of ovarian and prostate cancer cells (43,44).

Several observations led us to focus on p110β as a crucial mediator of the *Trp53;Pten*-null tumor phenotype. p110β has been shown to essential for tumorigenesis in a *PTEN*-null context (29,30). In addition, p110β can be activated by both RTKs and GPCRs but genetic data suggest a minor impact of p110β deletion, or its lipid kinase inactivation, on RTK signaling (21). *In vitro*, only a fraction of PTEN-null cancer cells are sensitive to p110β inhibitors and *in vivo* studies have not consistently shown tumor regression (45,46). As single-agent, the dual PI3K and mTOR inhibitor Apitolisib (GDC0980) showed modest antitumor activity in a phase I trial that included patients with advanced MM (47), indicating that PI3K inhibitors need to be combined with other drugs to achieve greater antitumor effects. The MAPK pathway activation observed in *Trp53;Pten*-null tumors pointed to the combination of p110β and MEK inhibitors. Indeed, we observed that p110β (TGX221) and MEK (PD325901) inhibitors show synergy on the growth of *Trp53;Pten*-null tumor cells. More importantly, the combination of two drugs that are currently under clinical investigation and target MEK and p110β revealed strong antitumor effect *in vivo* in established *Trp53;Pten*-null tumors, including induction of complete pathological responses. Several early-phase clinical studies using MEK and PI3K inhibitors are ongoing with significant toxicity (48), but we did not encounter toxicity in mice. Recent data point that the use of isoform-selective PI3K inhibitors would allow optimizing combined therapy and reducing toxicity (49). Accordingly, p110β/MEK inhibition has been proposed in preclinical settings for PTEN-deficient/*BRAF*-mutated melanoma (50).

One major reason for the inability to reproduce promising results of preclinical studies in clinical trials is the lack of adequate patient stratification. Here, we provide evidence pointing to the non-epithelioid histology and high Vimentin, AKT1/2, and Gαi2 protein levels as predictive markers of response to Selumetinib/AZD8186 therapy by testing this combination on 20 primary cultures derived from epithelioid, biphasic, and sarcomatoid human pl-MM. Responder cells presented significantly lower GI50s to combined therapy than cisplatin. We propose that this combination be tested in patients with advanced MM with biphasic/sarcomatoid features, a subgroup for which therapeutic options – including

surgery – are scarce. Should the acceptable toxicity observed in mice hold in patients, the combination of Selumetinib/AZD8186 with cisplatin would also merit consideration.

In summary, we identify a novel druggable molecular pathway driven by GPCRs/MEK/p110β signaling, which has a major impact on MM progression using human-relevant genetic mouse models and represents a novel targeted therapy for patients with MM whose tumors display sarcomatoid features.

Acknowledgements

We thank E. Andrada, N. Malats, M. Márquez, M. Rava, V. J. Sánchez-Arévalo Lobo, and F. Larousserie for valuable contributions; the Imaging and Histopathology CNIO Units for help with CT and histology interpretation; and M. Barbacid, R. García, X. Bustelo, A. C. Carrera, P. Smith, and A. Nebreda for valuable comments to earlier versions of the manuscript. AZ provided drug (as required by AZ publication policy).

Data and material availability

Raw and processed sequencing data are available in The Gene Expression Omnibus (GEO) repository (GSE138389).

BIBLIOGRAPHY

1. Yap TA, Aerts JG, Popat S, Fennell DA. Novel insights into mesothelioma biology and implications for therapy. Nat Rev Cancer **2017**;17:475-88
2. Zalcman G, Mazieres J, Margery J, Greillier L, Audigier-Valette C, Moro-Sibilot D, *et al.* Bevacizumab for newly diagnosed pleural mesothelioma in the Mesothelioma Avastin Cisplatin Pemetrexed Study (MAPS): a randomised, controlled, open-label, phase 3 trial. Lancet **2016**;387:1405-14
3. Christensen BC, Houseman EA, Poage GM, Godleski JJ, Bueno R, Sugarbaker DJ, *et al.* Integrated profiling reveals a global correlation between epigenetic and genetic alterations in mesothelioma. Cancer Res **2010**;70:5686-94
4. de Reynies A, Jaurand MC, Renier A, Couchy G, Hysi I, Elarouci N, *et al.* Molecular classification of malignant pleural mesothelioma: identification of a poor prognosis subgroup linked to the epithelial-to-mesenchymal transition. Clin Cancer Res **2014**;20:1323-34
5. Yoshikawa Y, Emi M, Hashimoto-Tamaoki T, Ohmuraya M, Sato A, Tsujimura T, *et al.* High-density array-CGH with targeted NGS unmask multiple noncontiguous minute deletions on chromosome 3p21 in mesothelioma. Proc Natl Acad Sci U S A **2016**;113:13432-7
6. Bueno R, Stawiski EW, Goldstein LD, Durinck S, De Rienzo A, Modrusan Z, *et al.* Comprehensive genomic analysis of malignant pleural mesothelioma identifies recurrent mutations, gene fusions and splicing alterations. Nat Genet **2016**;48:407-16
7. Hmeljak J, Sanchez-Vega F, Hoadley KA, Shih J, Stewart C, Heiman DI, *et al.* Integrative Molecular Characterization of Malignant Pleural Mesothelioma. Cancer Discov **2018**
8. Blum Y, Meiller C, Quetel L, Elarouci N, Ayadi M, Tashtanbaeva D, *et al.* Dissecting heterogeneity in malignant pleural mesothelioma through histo-molecular gradients for clinical applications. Nat Commun **2019**;10:1333
9. Altomare DA, You H, Xiao GH, Ramos-Nino ME, Skele KL, De Rienzo A, *et al.* Human and mouse mesotheliomas exhibit elevated AKT/PKB activity, which can be targeted pharmacologically to inhibit tumor cell growth. Oncogene **2005**;24:6080-9
10. Zhou S, Liu L, Li H, Eilers G, Kuang Y, Shi S, *et al.* Multipoint targeting of the PI3K/mTOR pathway in mesothelioma. Br J Cancer **2014**;110:2479-88
11. Kanteti R, Dhanasingh I, Kawada I, Lennon FE, Arif Q, Bueno R, *et al.* MET and PI3K/mTOR as a potential combinatorial therapeutic target in malignant pleural mesothelioma. PLoS One **2014**;9:e105919
12. Shukuya T, Serizawa M, Watanabe M, Akamatsu H, Abe M, Imai H, *et al.* Identification of actionable mutations in malignant pleural mesothelioma. Lung Cancer **2014**;86:35-40
13. Opitz I, Soltermann A, Abaecherli M, Hinterberger M, Probst-Hensch N, Stahel R, *et al.* PTEN expression is a strong predictor of survival in mesothelioma patients. Eur J Cardiothorac Surg **2008**;33:502-6
14. Agarwal V, Campbell A, Beaumont KL, Cawkwell L, Lind MJ. PTEN protein expression in malignant pleural mesothelioma. Tumour Biol **2013**;34:847-51
15. Cedres S, Ponce-Aix S, Pardo-Aranda N, Navarro-Mendivil A, Martinez-Marti A, Zugazagoitia J, *et al.* Analysis of expression of PTEN/PI3K pathway and programmed cell death ligand 1 (PD-L1) in malignant pleural mesothelioma (MPM). Lung Cancer **2016**;96:1-6

16. Garland LL, Rankin C, Gandara DR, Rivkin SE, Scott KM, Nagle RB, *et al.* Phase II study of erlotinib in patients with malignant pleural mesothelioma: a Southwest Oncology Group Study. J Clin Oncol **2007**;25:2406-13

17. Jongsma J, van Montfort E, Vooijs M, Zevenhoven J, Krimpenfort P, van der Valk M, *et al.* A conditional mouse model for malignant mesothelioma. Cancer Cell **2008**;13:261-71

18. Guo Y, Chirieac LR, Bueno R, Pass H, Wu W, Malinowska IA, *et al.* Tsc1-Tp53 loss induces mesothelioma in mice, and evidence for this mechanism in human mesothelioma. Oncogene **2014**;33:3151-60

19. Sementino E, Menges CW, Kadariya Y, Peri S, Xu J, Liu Z, *et al.* Inactivation of Tp53 and Pten drives rapid development of pleural and peritoneal malignant mesotheliomas. J Cell Physiol **2018**

20. Fruman DA, Chiu H, Hopkins BD, Bagrodia S, Cantley LC, Abraham RT. The PI3K Pathway in Human Disease. Cell **2017**;170:605-35

21. Guillermet-Guibert J, Bjorklof K, Salpekar A, Gonella C, Ramadani F, Bilancio A, *et al.* The p110beta isoform of phosphoinositide 3-kinase signals downstream of G protein-coupled receptors and is functionally redundant with p110gamma. Proc Natl Acad Sci U S A **2008**;105:8292-7

22. Suzuki A, Yamaguchi MT, Ohteki T, Sasaki T, Kaisho T, Kimura Y, *et al.* T cell-specific loss of Pten leads to defects in central and peripheral tolerance. Immunity **2001**;14:523-34

23. Jonkers J, Meuwissen R, van der Gulden H, Peterse H, van der Valk M, Berns A. Synergistic tumor suppressor activity of BRCA2 and p53 in a conditional mouse model for breast cancer. Nat Genet **2001**;29:418-25

24. Gao J, Aksoy BA, Dogrusoz U, Dresdner G, Gross B, Sumer SO, *et al.* Integrative analysis of complex cancer genomics and clinical profiles using the cBioPortal. Sci Signal **2013**;6:pl1

25. Amin W, Parwani AV, Melamed J, Flores R, Pennathur A, Valdivieso F, *et al.* National Mesothelioma Virtual Bank: A Platform for Collaborative Research and Mesothelioma Biobanking Resource to Support Translational Research. Lung Cancer Int **2013**;2013:765748

26. Chetram MA, Hinton CV. PTEN regulation of ERK1/2 signaling in cancer. J Recept Signal Transduct Res **2012**;32:190-5

27. Ou WB, Hubert C, Corson JM, Bueno R, Flynn DL, Sugarbaker DJ, *et al.* Targeted inhibition of multiple receptor tyrosine kinases in mesothelioma. Neoplasia **2011**;13:12-22

28. Burns DL. Subunit structure and enzymic activity of pertussis toxin. Microbiol Sci **1988**;5:285-7

29. Wee S, Wiederschain D, Maira SM, Loo A, Miller C, deBeaumont R, *et al.* PTEN-deficient cancers depend on PIK3CB. Proc Natl Acad Sci U S A **2008**;105:13057-62

30. Jia S, Liu Z, Zhang S, Liu P, Zhang L, Lee SH, *et al.* Essential roles of PI(3)K-p110beta in cell growth, metabolism and tumorigenesis. Nature **2008**;454:776-9

31. Tranchant R, Quetel L, Tallet A, Meiller C, Renier A, de Koning L, *et al.* Co-occurring mutations of tumor suppressor genes, LATS2 and NF2, in malignant pleural mesothelioma. Clin Cancer Res **2016**

32. Schelch K, Hoda MA, Klikovits T, Munzker J, Ghanim B, Wagner C, *et al.* Fibroblast growth factor receptor inhibition is active against mesothelioma and synergizes with radio- and chemotherapy. Am J Respir Crit Care Med **2014**;190:763-72

33. Hoda MA, Pirker C, Dong Y, Schelch K, Heffeter P, Kryeziu K, *et al.* Trabectedin Is Active against Malignant Pleural Mesothelioma Cell and Xenograft Models and Synergizes with Chemotherapy and Bcl-2 Inhibition In Vitro. Mol Cancer Ther **2016**;15:2357-69

34. Singh AS, Heery R, Gray SG. In Silico and In Vitro Analyses of LncRNAs as Potential Regulators in the Transition from the Epithelioid to Sarcomatoid Histotype of Malignant Pleural Mesothelioma (MPM). Int J Mol Sci **2018**;19

35. Jean D, Jaurand MC. Mesotheliomas in Genetically Engineered Mice Unravel Mechanism of Mesothelial Carcinogenesis. Int J Mol Sci **2018**;19

36. Laurie SA, Gupta A, Chu Q, Lee CW, Morzycki W, Feld R, *et al.* Brief report: a phase II study of sunitinib in malignant pleural mesothelioma. the NCIC Clinical Trials Group. J Thorac Oncol **2011**;6:1950-4

37. Song MS, Salmena L, Pandolfi PP. The functions and regulation of the PTEN tumour suppressor. Nat Rev Mol Cell Biol **2012**;13:283-96

38. Loffler MW, Steinhilber J, Hilke FJ, Haen SP, Bosmuller H, Montes-Mojarro IA, *et al.* First case report of malignant peritoneal mesothelioma and oral verrucous carcinoma in a patient with a germline PTEN mutation: a combination of extremely rare diseases with probable further implications. BMC Med Genet **2018**;19:144

39. Ujiie H, Kadota K, Nitadori JI, Aerts JG, Woo KM, Sima CS, *et al.* The tumoral and stromal immune microenvironment in malignant pleural mesothelioma: A comprehensive analysis reveals prognostic immune markers. Oncoimmunology **2015**;4:e1009285

40. Cornelissen R, Lievense LA, Maat AP, Hendriks RW, Hoogsteden HC, Bogers AJ, *et al.* Ratio of intratumoral macrophage phenotypes is a prognostic factor in epithelioid malignant pleural mesothelioma. PLoS One **2014**;9:e106742

41. Thapa B, Salcedo A, Lin X, Walkiewicz M, Murone C, Ameratunga M, *et al.* The Immune Microenvironment, Genome-wide Copy Number Aberrations, and Survival in Mesothelioma. J Thorac Oncol **2017**;12:850-9

42. Milella M, Falcone I, Conciatori F, Cesta Incani U, Del Curatolo A, Inzerilli N, *et al.* PTEN: Multiple Functions in Human Malignant Tumors. Front Oncol **2015**;5:24

43. Zhong M, Clarke S, Vo BT, Khan SA. The essential role of Gialpha2 in prostate cancer cell migration. Mol Cancer Res **2012**;10:1380-8

44. Fu X, Li Y, Alvero A, Li J, Wu Q, Xiao Q, *et al.* MicroRNA-222-3p/GNAI2/AKT axis inhibits epithelial ovarian cancer cell growth and associates with good overall survival. Oncotarget **2016**;7:80633-54

45. Ni J, Liu Q, Xie S, Carlson C, Von T, Vogel K, *et al.* Functional characterization of an isoform-selective inhibitor of PI3K-p110beta as a potential anticancer agent. Cancer Discov;2:425-33

46. Weigelt B, Warne PH, Lambros MB, Reis-Filho JS, Downward J. PI3K pathway dependencies in endometrioid endometrial cancer cell lines. Clin Cancer Res;19:3533-44

47. Dolly SO, Wagner AJ, Bendell JC, Kindler HL, Krug LM, Seiwert TY, *et al.* Phase I Study of Apitolisib (GDC-0980), Dual Phosphatidylinositol-3-Kinase and Mammalian Target of Rapamycin Kinase Inhibitor, in Patients with Advanced Solid Tumors. Clin Cancer Res **2016**;22:2874-84

48. Bedard PL, Tabernero J, Janku F, Wainberg ZA, Paz-Ares L, Vansteenkiste J, *et al.* A phase Ib dose-escalation study of the oral pan-PI3K inhibitor buparlisib (BKM120) in combination with

the oral MEK1/2 inhibitor trametinib (GSK1120212) in patients with selected advanced solid tumors. Clin Cancer Res **2015**;21:730-8

49. van Geel R, Tabernero J, Elez E, Bendell JC, Spreafico A, Schuler M, *et al.* A Phase Ib Dose-Escalation Study of Encorafenib and Cetuximab with or without Alpelisib in Metastatic BRAF-Mutant Colorectal Cancer. Cancer Discov **2017**;7:610-9

50. Bonnevaux H, Lemaitre O, Vincent L, Levit MN, Windenberger F, Halley F, *et al.* Concomitant Inhibition of PI3Kbeta and BRAF or MEK in PTEN-Deficient/BRAF-Mutant Melanoma Treatment: Preclinical Assessment of SAR260301 Oral PI3Kbeta-Selective Inhibitor. Mol Cancer Ther **2016**;15:1460-71

Figure Legends

Figure 1. Mesothelial-specific inactivation of *Pten* and *Trp53* results in SMM development. **A**, Schematic representation of the conditional targeting of the *Pik3ca*^{H1047R} mutation in the endogenous *Pik3ca* locus. **B,** H&E staining of a mesothelioma from an adeno-Cre inoculated *Pten;Trp53*-null mouse growing extrinsically to the bladder wall. Scale bar, 200μm (left), 50μm (right). **C,** Adult *Rosa26-LSL-LacZ* mice were inoculated with either PBS or adeno-Cre in the bladder and stained for βGal activity 2 weeks after injection. Scale bar, 200μm (left), 50μm (right). **D,** H&E staining of a *Pten;Trp53*-null SMM invading fat (left) and muscle (right). Scale bar, 100μm. **E,** H&E and immunohistochemical analysis of the expression of the indicated proteins in representative sections of tumors from *Pten;Trp53*-null and *Pik3ca**;Trp53*-null mice. Scale bar, 50μm. **F,** Kaplan-Meier survival curves of mice of the indicated genotypes injected with adeno-Cre and monitored prospectively; ****P*<0.001, Log-rank (Mantel-Cox) test.

Figure 2. *Pten;Trp53*-null MMs exhibit an immunosuppressive stroma. **A**, Representative cleaved-Caspase 3 and phospho-Histone 3 staining images of *Pten;Trp53*-null and *Pik3ca**;Trp53*-null tumors. Scale bar, 50μm. **B, C**, Normalized DAB signal of staining of the indicated markers in *Pten;Trp53*-null and *Pik3ca**;Trp53*-null mouse tumors. Graphs show mean±SEM. **P*<0.05, ***P*<0.01, Mann-Whitney U-Test. **D**, Representative images of immunohistochemical analysis of the indicated immune components in *Pten;Trp53*-null and *Pik3ca**;Trp53*-null tumors. Scale bar, 50μm. **E**, PD-L1 and Ppib RNAscope analysis in *Pten;Trp53*-null and *Pik3ca**;Trp53*-null MMs. Representative sections are shown. **F**, Graphs show mean±SEM of Ppib-normalized PD-L1 RNAscope signal in *Pten;Trp53*-null and *Pik3ca**;Trp53*-null tumors. **P*<0.05, ***P*<0.01, Mann-Whitney U-Test.

Figure 3. Human SMM tumor samples display low PTEN expression. **A,** Representative PTEN immunohistochemistry staining displaying strong (upper-left panel), moderate (upper-right panel), low (lower-right) and no staining (lower-left), Scale bar, 50μm. **B,** Bar graph representing the proportion of cases scored as PTEN-positive and PTEN-negative tumors with epithelioid (n=122), biphasic (n=20), and sarcomatoid (n=7) features. **C,** Box plot representing PTEN histoscores in the epithelioid (n=122), biphasic (n=20) and sarcomatoid (n=7) tumor subgroups. **P*<0.05, Tukey post-hoc test. **D-E,** Box plot representing indicated gene mRNA normalized counts in transcriptomically defined (D, upper panels) and histological subtypes (D, lower panels) from Bueno *et al.* (**D**) and TCGA (**E**) cohorts. **P*<0.05, ***P*<0.01, ****P*<0.001 Tukey post-hoc test.

Figure 4. *Pten* inactivation results in tumors with strong Mek/Erk activation, involved in tumor cell proliferation and *in vitro* invasiveness. **A, B,** WB analysis of the indicated proteins using lysates of tumors from adeno-Cre inoculated *Pten;Trp53*-null and *Pik3ca*;Trp53*-null mice. **C,** Densitometric quantitation of signal intensity of phosphorylated proteins normalized to total protein (pAkt/Akt, pErk1/2 / Erk1/2, pMek1/2 / Mek1/2) using ImageJ software. Graphs show mean±SEM; **P*<0.05, ***P*<0.01, Mann-Whitney U-Test. **D,** Phase contrast images of cultures established from *Pten;Trp53*-null and *Pik3ca*;Trp53*-null tumors. **E,** WB analysis from a representative experiment (n=4) of the indicated proteins using total lysates of exponentially growing *Pten;Trp53*-null and *Pik3ca*;Trp53*-null MM cells. **F,** Effects of PD325901 (0.5 μM) on the proliferation of *Pten;Trp53*-null and *Pik3ca*;Trp53*-null MM cells. Graphs show mean ± SEM of fold-increase in cell number with respect to the 0 h time point (n=4 independent experiments). **P*<0.05, Mann-Whitney U-Test. **G,** Effects of PD325901 (0.5 μM) on the *in vitro* invasion of *Pten;Trp53*-null and *Pik3ca*;Trp53*-null MM cells assessed after 48 h. Invading and non-invading cells were visualized by confocal microscopy. Graphs show mean ± SEM of the % of invading cells per field (n=4 independent experiments). **P*<0.05, Mann-Whitney U-Test.

Figure 5. **Gαi2 signaling mediates pErk and pAkt levels in *Pten;Trp53*-null MM. A,** Phospho-RTK dot blot array analysis using lysates of tumors from adeno-Cre inoculated *Pten;Trp53*-null and *Pik3ca*;Trp53*-null mice. Phospho-receptors showing differences in signal intensity between both genotypes are highlighted: #1, Erbb4; #2, Fgfr3; #3, Scfr; #4, Flt-3; #5, EphB1. **B,** The heatmap shows ImageJ software signal quantification of all the RTK included in the array. **C,** Effects of PTX 100ng/ml (15h) on signaling in *Pten;Trp53*-null and *Pik3ca*;Trp53*-null MM cells. Cell lysates were analyzed by WB with the indicated antibodies. Representative results of ≥3 independent experiments. **D,** Boxplots of log10-transformed normalized count values for each Gαi gene in *Pten;Trp53*-null and *Pik3ca*;Trp53*-null tumors. **E,** Immunohistochemical analysis of Gαi2 expression in representative sections of tumors from *Pten;Trp53*-null and *Pik3ca*;Trp53*-null mice. Scale bar, 50μm. **F,** WB analysis from a representative experiment (n=2) of the indicated proteins using total lysates of exponentially growing *Pten;Trp53*-null and *Pik3ca*;Trp53*-null MM cells infected either with non-targeting (Nt) or Gαi2-targeting shRNAs. **G,** Box plot representing GNAI2 RNAseq normalized counts of transcriptomically defined (left) and histological (right) subtypes from Bueno et al. sample cohort.

Figure 6. **Selumetinib and AZD8186 synergize to impair the *in vivo* growth of *Pten;Trp53*-null MM**. **A,** Effects of PD325901 (0.5μM), TGX-221 (10μM), and their combination (PD+TGX) on the

proliferation of *Pten;Trp53*-null MM cells. Graphs show mean ± SEM of fold-increase with respect to the 0 h time point (n=3-5 independent experiments). P*<0.05, Mann-Whitney U-Test. **B,** Effects of PD325901 (0.5μM), TGX-221 (10μM), and their combination (PD+TGX) on the *in vitro* invasion of *Pten;Trp53*-null MM cells assessed at 24h. Graphs show mean ± SEM of the % of invading cells per field in the different conditions (n=4 independent experiments). **P*<0.05, ***P*<0.01, Mann-Whitney U-Test. **C,** Representative H&E stainings of *Pten;Trp53*-null SMM displaying bone differentiation (left panel, Scale bar, 50μm) and *Pten;Trp53*-null SMM 6 weeks after adeno-Cre inoculation (right panel, Scale bar, 200μm). **D,** Kaplan-Meier survival curves of *Pten;Trp53*-null tumor-bearing mice treated for 7 weeks with vehicle, Selumetinib (10mg/kg), AZD8186 (40mg/kg) or both (S+AZD) (n=6/group). **P*<0.05, Log-rank (Mantel-Cox) test. **E,** Representative axial micro-CT images of the abdomen of adeno-cre inoculated *Pten;Trp53*-null mice before and 1-3 weeks after treatment. Arrows indicate the bladder; tumors (with bone differentiation signal) are indicated by an asterisk. Thickening of the abdominal wall is shown as an arrowhead. **F,** Kaplan-Meier survival curves of *Pten;Trp53*-null tumor-bearing mice treated for 12 weeks with vehicle, or both (S+AZD, 10mg/kg Selumetinib, 40mg/kg AZD8186) (n=11/group). ***P*<0.01, Log-rank (Mantel-Cox) test.

Figure 7. The Selumetinib/AZD8186 combination inhibits proliferation of primary human cultures derived from non-epithelioid human pl-MM harboring *TP53* mutations. **A,** Graphs show % cell viability ± SEM (n=2-3) after 72h of exposure to serial drug dilutions or to the drug combination (S+AZD) at a constant ratio for Selumetinib/AZD8186 responder cells. Compound concentrations range from 0.025 to 20μM. The combination ratios for Selumetinib and AZD8186 used for each specific cell line are specified in Supplementary Table S3. **B,** The heatmap shows normalized AUC values for serial dilutions of the indicated compounds, representing drug response of each human MPM primary culture. Original tumor histology of the cell lines is indicated. **C,** Normalized AUC for Selumetinib, AZD8186 or the combination (S+AZD), for cultures derived from EMM, BMM, and SMM. **P*<0.05, Mann-Whitney U-Test. **D,** WB analysis of the indicated proteins using lysates of primary human MM cultures. Original tumor histology of the cell lines, TP53 status and normalized AUC are also indicated **E**, The heatmap represents unsupervised clusterization of human primary MPM cells based on densitometric ImageJ software quantitation of WB signal intensities of Gαi2, Vimentin, and AKT1/2 proteins normalized to Vinculin. Normalized AUC values of each cell line are also indicated. **F,** GI50 values for cisplatin and for Selumetinib/AZD8186 (S+AZD) for combination-responder cells and combination non-responder cells**.**

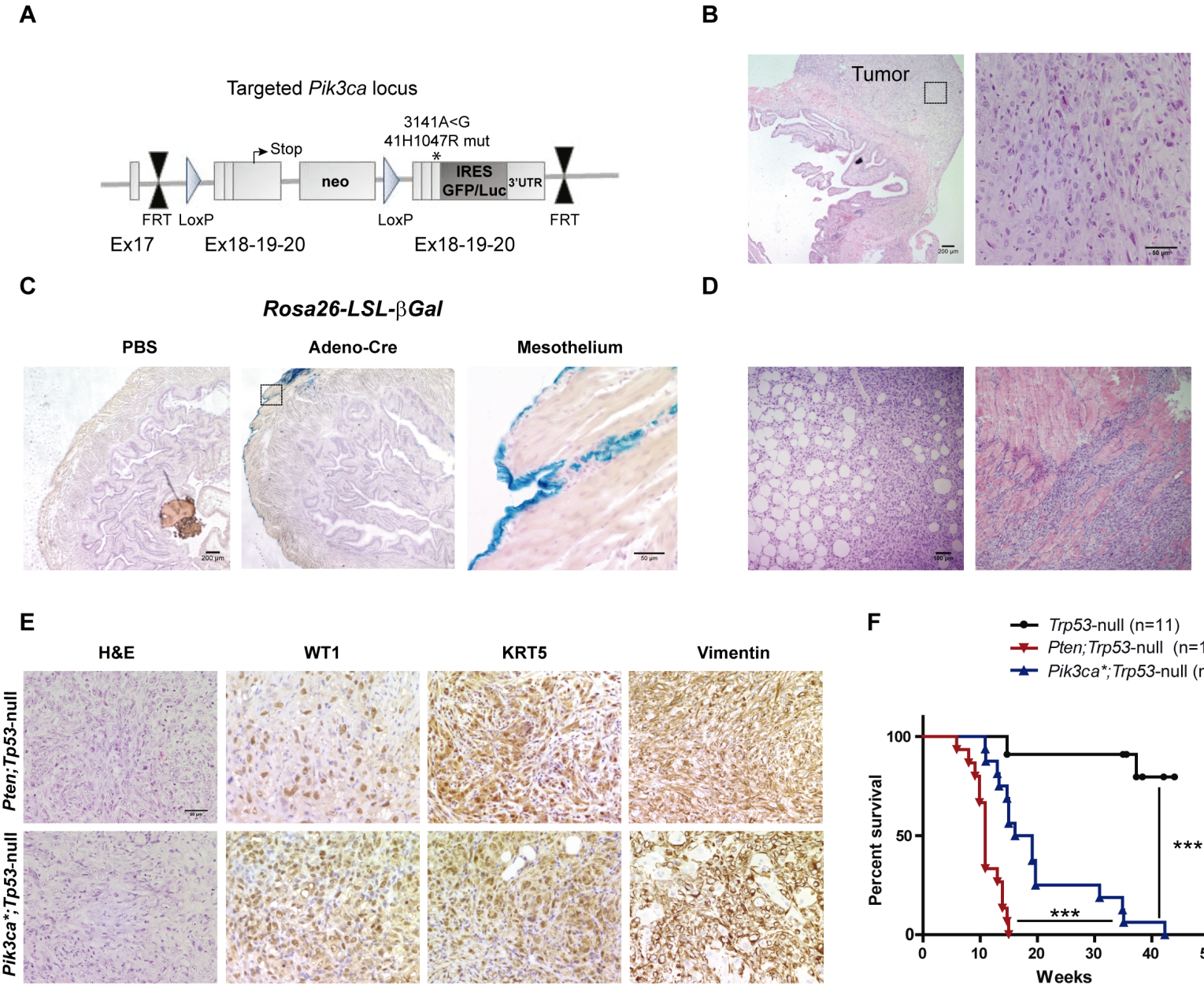
A
Targeted Pik3ca locus
3141A<G
41H1047R mut
Stop
neo
IRES
GFP/Luc
3'UTR
FRT
LoxP
LoxP
FRT
Ex17
Ex18-19-20
Ex18-19-20
B
Tumor
C
Rosa26-LSL-βGal
PBS
Adeno-Cre
Mesothelium
D
E
H&E
WT1
KRT5
Vimentin
Pten;Tp53-null
Pik3ca*;Tp53-null
F
Trp53-null (n=11)
Pten;Trp53-null (n=10)
Pik3ca*;Trp53-null (n=15)
Percent survival
Weeks
***
***

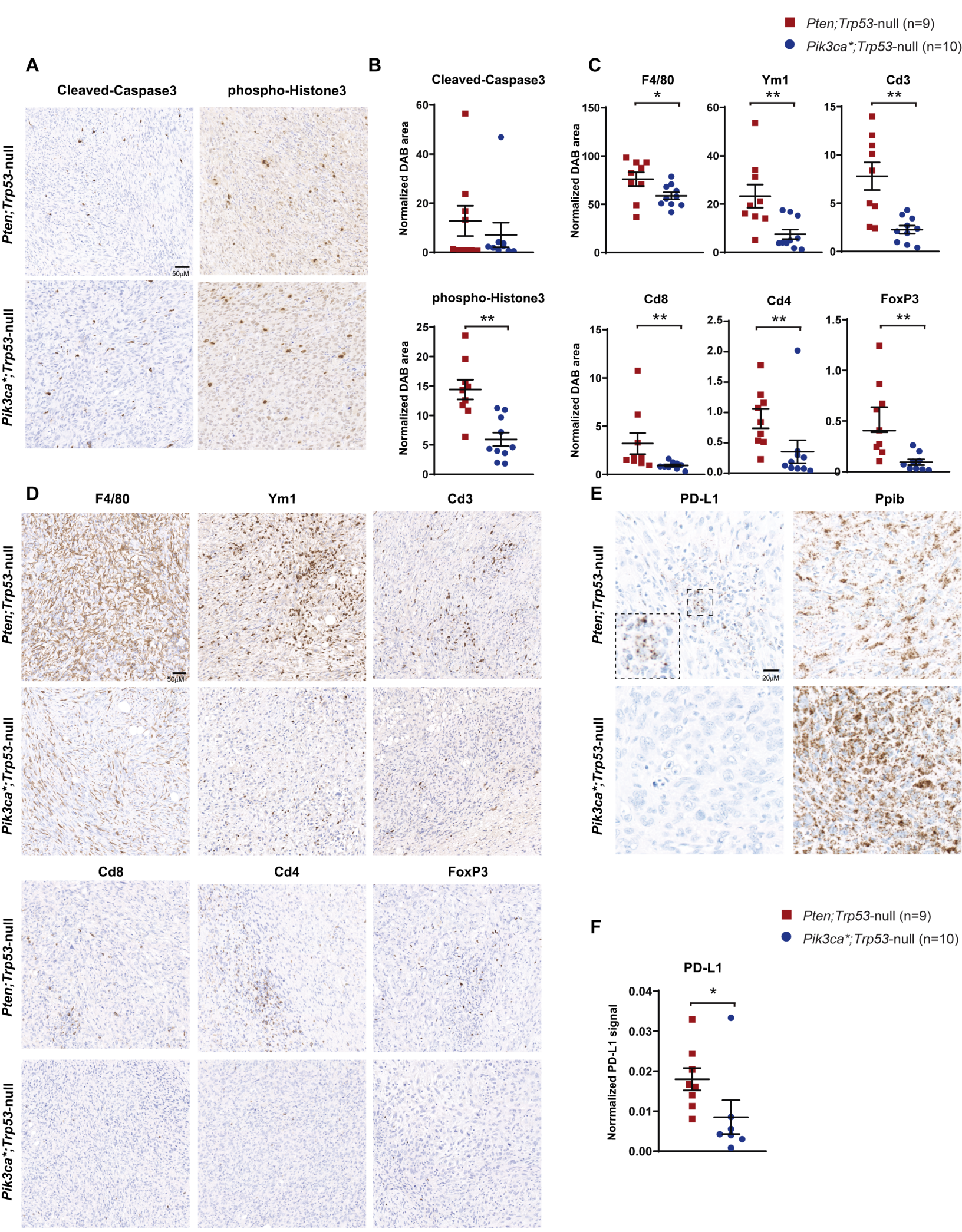
Pten;Trp53-null (n=9)
Pik3ca*;Trp53-null (n=10)
A
Cleaved-Caspase3
phospho-Histone3
Pten;Trp53-null
Pik3ca*;Trp53-null
50μM
B
Cleaved-Caspase3
Normalized DAB area
phospho-Histone3
**
C
F4/80
Ym1
Cd3
Cd8
Cd4
FoxP3
*
**
D
F4/80
Ym1
Cd3
Cd8
Cd4
FoxP3
E
PD-L1
Ppib
20μM
F
PD-L1
Normalized PD-L1 signal

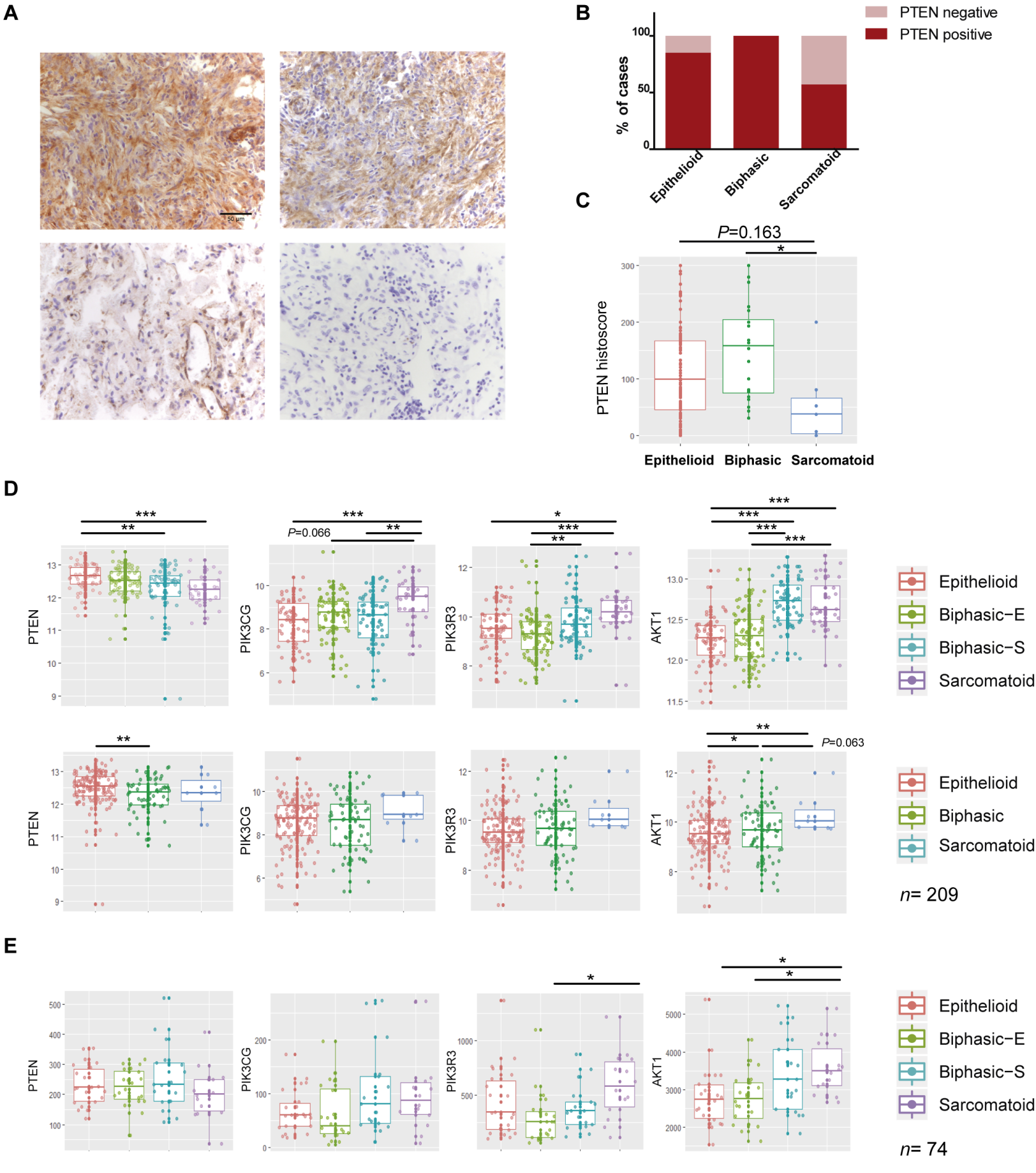
A
50 μm
B
PTEN negative
PTEN positive
% of cases
100
50
0
Epithelioid
Biphasic
Sarcomatoid
C
P=0.163
*
PTEN histoscore
300
200
100
0
Epithelioid
Biphasic
Sarcomatoid
D
PTEN
PIK3CG
PIK3R3
AKT1
P=0.066
P=0.063
Epithelioid
Biphasic−E
Biphasic−S
Sarcomatoid
Biphasic
n= 209
E
n= 74

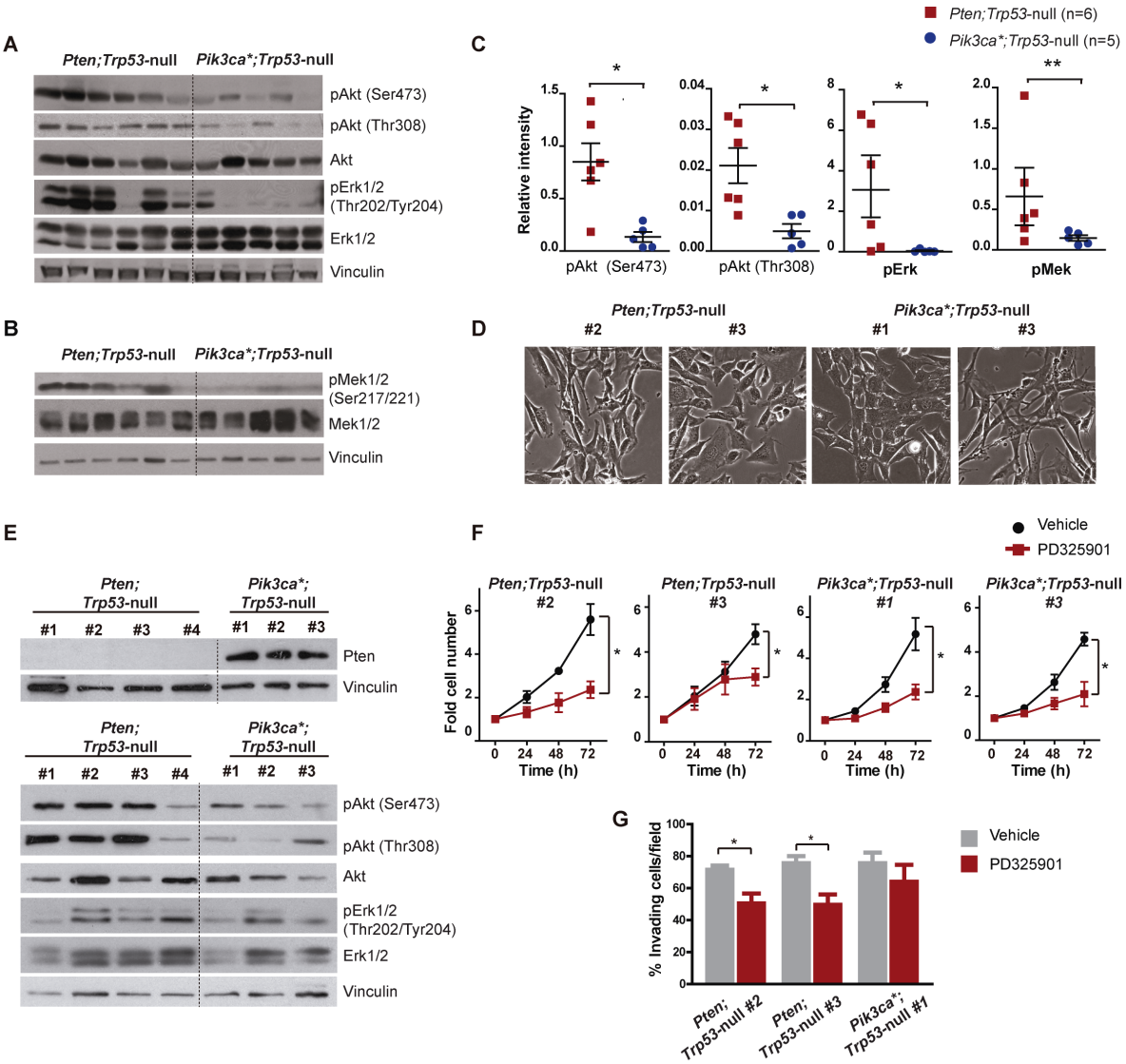
A
Pten;Trp53-null
Pik3ca*;Trp53-null
pAkt (Ser473)
pAkt (Thr308)
Akt
pErk1/2 (Thr202/Tyr204)
Erk1/2
Vinculin
B
Pten;Trp53-null
Pik3ca*;Trp53-null
pMek1/2 (Ser217/221)
Mek1/2
Vinculin
C
Pten;Trp53-null (n=6)
Pik3ca*;Trp53-null (n=5)
Relative intensity
pAkt (Ser473)
pAkt (Thr308)
pErk
pMek
D
Pten;Trp53-null
Pik3ca*;Trp53-null
#2
#3
#1
#3
E
Pten; Trp53-null
Pik3ca*; Trp53-null
#1 #2 #3 #4
#1 #2 #3
Pten
Vinculin
pAkt (Ser473)
pAkt (Thr308)
Akt
pErk1/2 (Thr202/Tyr204)
Erk1/2
Vinculin
F
Vehicle
PD325901
Pten;Trp53-null #2
Pten;Trp53-null #3
Pik3ca*;Trp53-null #1
Pik3ca*;Trp53-null #3
Fold cell number
Time (h)
G
% Invading cells/field
Vehicle
PD325901
Pten; Trp53-null #2
Pten; Trp53-null #3
Pik3ca*; Trp53-null #1

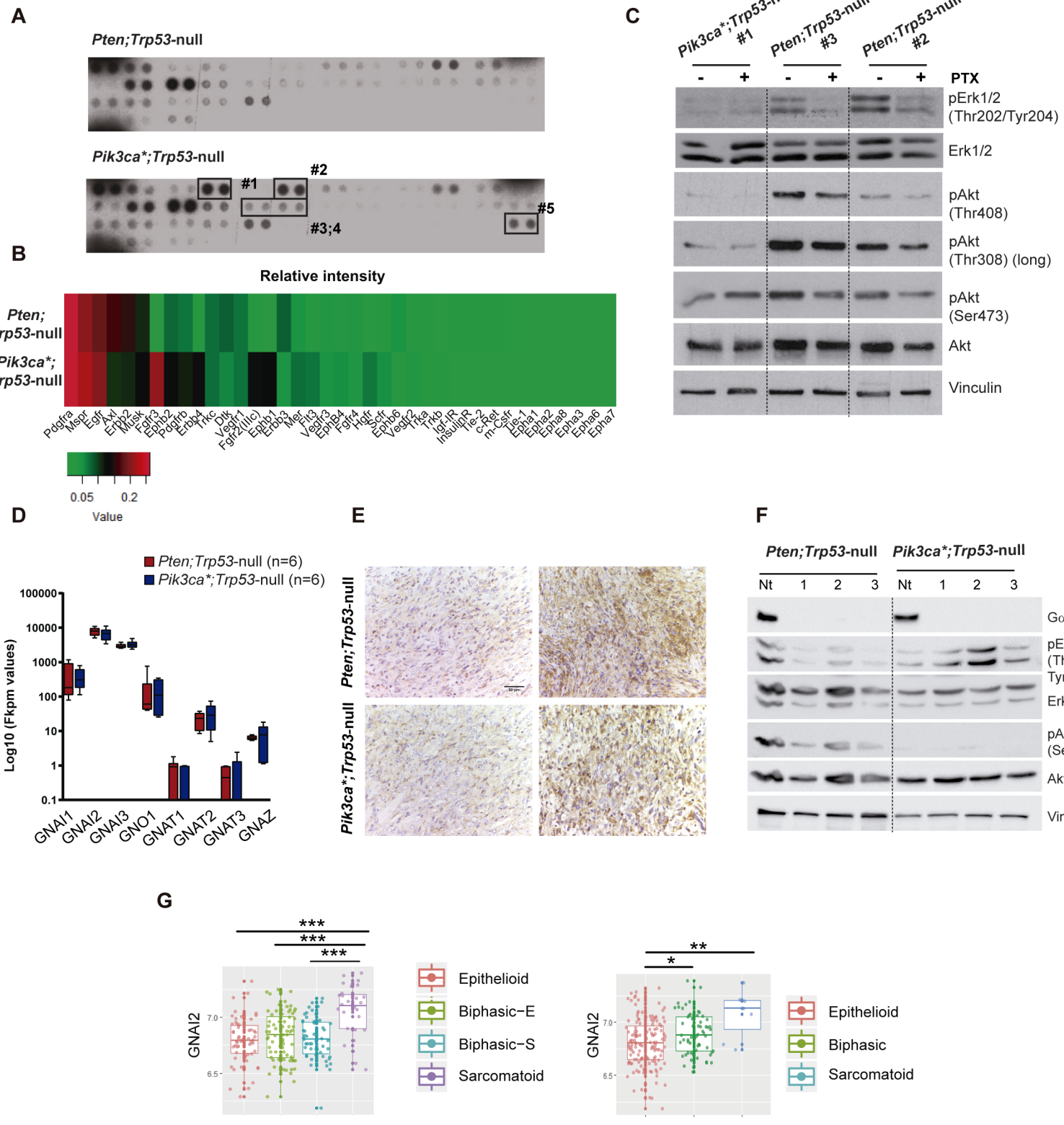
A
Pten;Trp53-null
Pik3ca*;Trp53-null
#1
#2
#3;4
#5
B
Relative intensity
Pten; Trp53-null
Pik3ca*; Trp53-null
Pdgfra Mspr Egfr Axl Erbb2 Musk Fgfr3 Ephb2 Pdgfrb Erbb4 Trkc Dtk Vegfr1 Fgfr2(IIIc) Ephb1 Erbb3 Mer Flt3 Vegfr3 EphB4 Fgfr4 Hgfr Scfr Ephb6 Vegfr2 Trka Trkb Igf-IR InsulinR Tie-2 c-Ret m-Csfr Tie-1 Epha1 Epha2 Epha8 Epha3 Epha6 Epha7
0.05 0.2
Value
C
Pik3ca*;Trp53-null #1
Pten;Trp53-null #3
Pten;Trp53-null #2
- + - + - +
PTX
pErk1/2 (Thr202/Tyr204)
Erk1/2
pAkt (Thr408)
pAkt (Thr308) (long)
pAkt (Ser473)
Akt
Vinculin
D
Pten;Trp53-null (n=6)
Pik3ca*;Trp53-null (n=6)
Log10 (Fkpm values)
100000 10000 1000 100 10 1 0.1
GNAI1 GNAI2 GNAI3 GNO1 GNAT1 GNAT2 GNAT3 GNAZ
E
Pten;Trp53-null
Pik3ca*;Trp53-null
F
Pten;Trp53-null
Pik3ca*;Trp53-null
Nt 1 2 3 Nt 1 2 3
Gαi2
pErk1/2 (Thr202/ Tyr204)
Erk1/2
pAkt (Ser473)
Akt
Vinculin
G
***
***
***
GNAI2
7.0
6.5
Epithelioid
Biphasic−E
Biphasic−S
Sarcomatoid
**
*
GNAI2
7.0
6.5
Epithelioid
Biphasic
Sarcomatoid

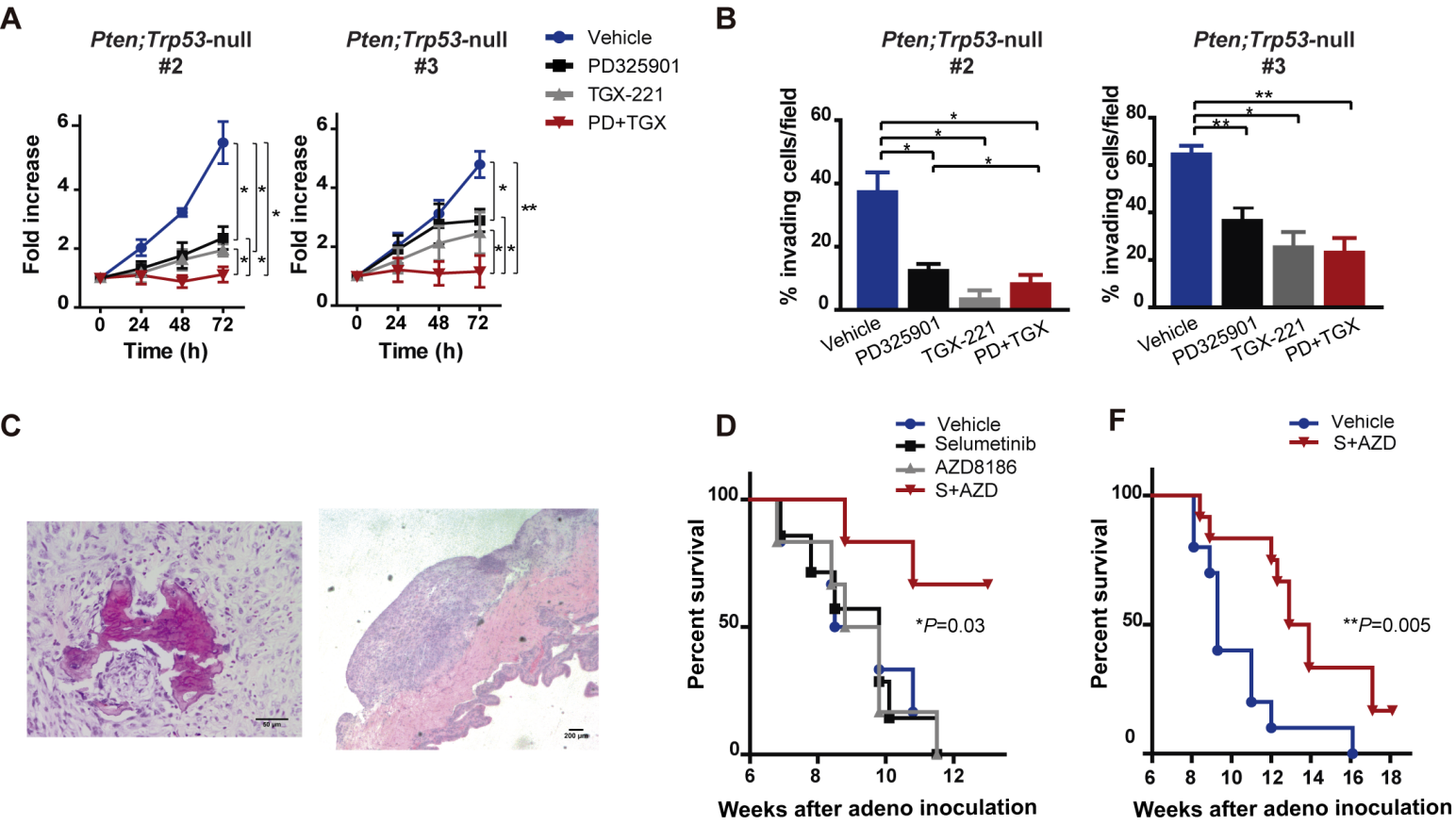
A
Pten;Trp53-null #2
Pten;Trp53-null #3
Vehicle
PD325901
TGX-221
PD+TGX
Fold increase
Time (h)
B
Pten;Trp53-null #2
Pten;Trp53-null #3
% invading cells/field
Vehicle
PD325901
TGX-221
PD+TGX
C
D
Vehicle
Selumetinib
AZD8186
S+AZD
Percent survival
*P=0.03
Weeks after adeno inoculation
F
Vehicle
S+AZD
Percent survival
**P=0.005
Weeks after adeno inoculation
E
Control
Selumetinib
AZD8186
S+AZD
pre-treatment
1 week
3 weeks

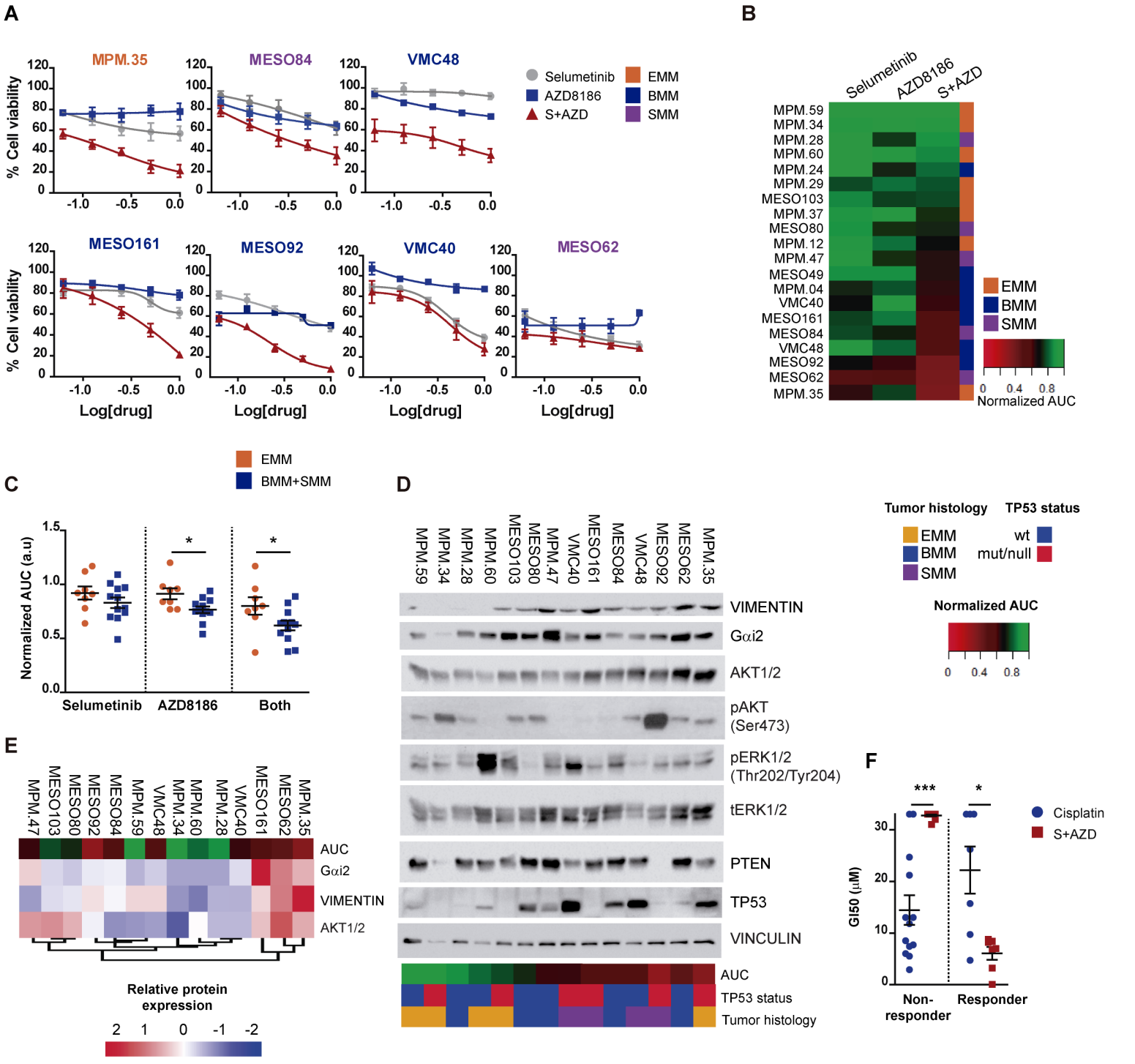
A
MPM.35
MESO84
VMC48
MESO161
MESO92
VMC40
MESO62
% Cell viability
Log[drug]
Selumetinib
AZD8186
S+AZD
EMM
BMM
SMM
B
Selumetinib
AZD8186
S+AZD
MPM.59
MPM.34
MPM.28
MPM.60
MPM.24
MPM.29
MESO103
MPM.37
MESO80
MPM.12
MPM.47
MESO49
MPM.04
VMC40
MESO161
MESO84
VMC48
MESO92
MESO62
MPM.35
EMM
BMM
SMM
0 0.4 0.8
Normalized AUC
C
EMM
BMM+SMM
Normalized AUC (a.u)
Selumetinib
AZD8186
Both
D
MPM.59
MPM.34
MPM.28
MPM.60
MESO103
MESO80
MPM.47
VMC40
MESO161
MESO84
VMC48
MESO92
MESO62
MPM.35
VIMENTIN
Gαi2
AKT1/2
pAKT (Ser473)
pERK1/2 (Thr202/Tyr204)
tERK1/2
PTEN
TP53
VINCULIN
AUC
TP53 status
Tumor histology
Tumor histology
EMM
BMM
SMM
TP53 status
wt
mut/null
Normalized AUC
0 0.4 0.8
E
MPM.47
MESO103
MESO80
MESO92
MESO84
MPM.59
VMC48
MPM.34
MPM.60
MPM.28
VMC40
MESO161
MESO62
MPM.35
AUC
Gαi2
VIMENTIN
AKT1/2
Relative protein expression
2 1 0 -1 -2
F
***
*
GI50 (μM)
Cisplatin
S+AZD
Non-responder
Responder